J Mater Sci (2010) 45:2580–2590
DOI 10.1007/s10853-010-4229-6

Modelling of microstructure evolution during hot rolling of a high-Nb HSLA steel

Yun Bo Xu · Yong Mei Yu · Bao Liang Xiao · Zhen Yu Liu · Guo Dong Wang

Received: 5 October 2009 / Accepted: 11 January 2010 / Published online: 29 January 2010

Abstract The microstructure evolution during thermo-mechanical processing of high-Nb HSLA steel has been investigated with laboratory investigations. Using the Gleeble 2000 thermomechanical simulator, constitutive behavior, recrystallization, and precipitation were quantified with single- and double-hit tests as well as isothermal-deformation-quenching tests. The critical strain (ε_c) for the onset of dynamic recrystallization in high-Nb steel is derived and the result shows that the critical strain/peak strain ratio is as low as approximately 0.35 and tends to a constant when the effective Nb content ($Nb_{eff} = Nb - Mn/120 + Si/94$) ranges from 0.07 to 0.10. The interaction between the recrystallization and precipitation was considered to determine non-recrystallization temperature (T_{nr}) under various conditions and further the dependence of the T_{nr} on initial austenite grain size, strain, and strain rate on was formulated.

Introduction

The advance in modern pipeline technology leads to the significant change of its final microstructure from a traditional ferrite-pearlite structure to an acicular ferrite-dominated structure. Alloy additions such as Mn, Nb, V, Ti, and Mo are commonly added to obtain the desired microstructure and mechanical properties, and particularly for Mo addition, it is usually regarded as an important element for the formation of acicular ferrite. Thus far, most works concerning acicular ferrite steels have been carried out on the relationship between microstructural features and mechanical properties in Mo-containing pipeline steels [1–11]. However, for Mo-containing steels, there are also some inherent metallurgical disadvantages such as the high alloying cost, large mill load, and low production efficiency due to low temperature heavy deformation in non-recrystallization region of austenite. On the other hand, we know, a large amount of Nb dissolved in austenite could exert a similar effect with Mo element by enhancing the austenite to acicular ferrite transformation with no or few formation of polygonal ferrite [12, 13]. In addition, the addition of Nb broadens austenite's non-recrystallization region through retarding static and dynamic recrystallization (DRX) [14]. Thus, driven by economic benefits, some steel makers have recently adopted a new high-Nb microalloying technology for high-strength pipeline steels, which allows Nb content up to 0.1% in steels and using high temperature process (HTP) technology in rolling [15, 16]. This HTP-technology, as a feasible alternative to the conventional Mo-alloying method in high-grade pipeline steels, enormously reduce alloying cost, lighten mill load, and is showing a very good development trend and prospect.

In order to make an effective use of alloying elements and to design optimized processing routes, it is necessary to gain a detailed knowledge of the essential metallurgical phenomena, i.e., recrystallization, precipitation, austenite grain growth, etc. A number of microstructural evolution models have been developed for hot rolling over the last two decades and validated for various steels including low-Nb (e.g., smaller than 0.06% in wt%) microalloying steels

Y. B. Xu (✉) · B. L. Xiao · Z. Y. Liu · G. D. Wang
State Key Laboratory of Rolling Technology and Automation, Northeastern University, P.O. Box 105, 110004 Shenyang, People's Republic of China
e-mail: xuyunbo@mail.neu.edu.cn

Y. M. Yu
Mechanical Engineering School, Shenyang University of Chemical Technology, 110142 Shenyang, People's Republic of China
e-mail: yongmei_yu@126.com

[17–24]. However, the development of these models for other high-strength low-alloy (HSLA) steels with Nb content as high as 0.1 (in wt%) is nearly in its infancy. The objective of the present investigation is to extend this microstructure modelling work to high-Nb HSLA steels. In these steels with greatly increased Nb additions, recrystallization may be inhibited such that retained strain intensely accumulates during finish rolling. Further, how to ensure sufficient solute Nb left in austenite are most significant for developing the desired fine-grained acicular ferrite microstructure as a result of the austenite decomposition. Thus, it is required to detailedly understand the characteristics of recrystallization and precipitation in these steels and to evaluate the extent to which the models previously proposed for low carbon low Nb steels remain applicable.

In the present work, constitutive behavior, DRX, static recrystallization (SRX), and precipitation of high-Nb HSLA steel have been investigated for hot-strip rolling. In order to formulate these metallurgical behaviors, single and double hit as well as isothermal-deformation-quenching tests have been conducted, respectively. Constitutive equations, recrystallization models, and strain-induced precipitation equations have been developed based on the experimental results. These models can permit the quantitative description of the recrystallization kinetics, recrystallized grain size, and precipitation behavior in the present steel. The interaction between the recrystallization and precipitation was considered to determine non-recrystallization temperature (T_{nr}) under various conditions and further the effects of initial austenite grain size, strain, and strain rate on the T_{nr} were quantified.

Material and experimental procedures

Material

The HTP pipeline steel used in this study was prepared in a 120-kg vacuum induction melted furnace, and the cast ingots were forged to slabs of 100 mm × 110 mm × 100 mm. Table 1 shows the chemical composition of the present steel. Notably, in steel A the Nb content is 0.1% and there is no Mo addition, i.e., it is significantly different from that of a conventional pipeline steel grade with predominantly Mo microalloying. In addition, by decreasing carbon content, i.e., less than 0.05 wt%, more amounts of Nb precipitates can be dissolved in austenite during reheating.

Table 1 Chemical composition of the tested steels (mass%)

Steel	C	Si	Mn	P	S	Al	Nb	N
A	0.024	0.17	1.49	0.006	0.0020	0.027	0.10	≤0.0036
B	0.067	0.20	1.18	0.006	0.0015	0.058	0.08	≤0.0040
C	0.053	0.16	1.18	0.004	0.0012	0.042	0.05	≤0.0040
D	0.072	0.23	1.60	0.004	0.0018	0.032	0.02	≤0.0040

Experimental procedures

In order to examine microstructural detail, laboratory tests were conducted on a Gleeble 2000 thermo-mechanical simulator including austenite grain growth, single- and double-hit tests. Solution treatment for 3 min at 1250 °C and quenching were applied to dissolve possible precipitates prior to the following tests. The austenite grain growth tests were carried out to determine reasonable austenitization conditions for subsequent deformation and recrystallization studies that require different initial austenite grain sizes. In this study, cylindrical specimens of 6- or 8-mm diameter and 15-mm length were rapidly heated to reheating temperatures in the range of 1000–1200 °C followed by holding for selected times (3 or 2 min) before quenching to reveal the prior austenite microstructure using etching and optical microscopy. The average linear intercept grain size was measured for at least 10 random fields using computer aided image analysis to describe the effect of initial grain size on recrystallization kinetics.

Single- and double-hit tests were performed in axisymmetric compression employing cylindrical specimens (ϕ 8 mm × 15 mm). Following austenitization, specimens were cooled at 10 °C/s to the deformation temperature, where they were held for 30 s to homogenize the temperature distribution in the specimens, which were then deformed at temperatures in the range of 900–1200 °C and at strain rates in the range of 0.1–10 s^{-1}. In single hit tests the applied strain was 1.

In double-hit tests, the deformation temperature range was from 900 to 1000 °C, the stain rate was 5 s^{-1}, and the pre-strain was about 0.3 and/or 0.5. After the first deformation, the compressive stress was relaxed and the samples were held for a selected time in the range of 1–400 s before they were deformed again under the same temperature and strain rate conditions as in the first hit. Additionally, after the first deformation and different times of holding, other specimens were quenched using water sprays to observe the austenite microstructure and strain-induced precipitation behavior. Noting that, solution treatment and austentizing conditions may ensure that there is no or little precipitation before deformation, and here we can assume that almost all the niobium is in solid state prior to double tests.

A combination of the optical microscopy and transmission electron microscopy (TEM) were employed in determining the microstructures of the specimens. The specimens for metallographic analysis were mechanically polished and etched with a 3% Nital solution, and then observed using optical microscopy. For TEM observation,

the thin foils were mechanically thinned from 300 to 50 μm, and then electropolished by a twin-jet electropolisher in a solution of 10% perchloric acid and 90% acetic acid. The thin foil specimens were observed using H-800 TEM with 200 kV.

Results and discussion

Austenite grain evolution

The initial austenite grain size has a significant influence on flow stress, recrystallization, and transformation kinetics. In the laboratory tests, austenite grain size can be changed by adopting various austenitization treatments. A series of reheating tests were thus carried out to obtain suitable initial austenite microstructures for subsequent recrystallization study. Figure 1 shows the austenite grain size of steel A as a function of reheating temperature for isochronal tests with holding times of 2 and/or 3 min.

Increasing the temperature from 950 to 1200 °C raises the linear intercept grain size from 12 to 64 μm for a holding time of 3 min, whereas there is no evident change from 950 to 1000 °C for a holding time of 2 min. That is to say, there is no apparent grain coarsening being observed at soaking temperatures of 1200 °C and below. This behavior should be attributed to the precipitation of microalloy carbonitride in this temperature range.

Constitutive behavior

Single hit tests were performed to investigate the constitutive behavior of the present steels (steel A–D). The typical stress–strain curves are shown in Fig. 2, which were determined at temperatures in the range of 850–1100 °C

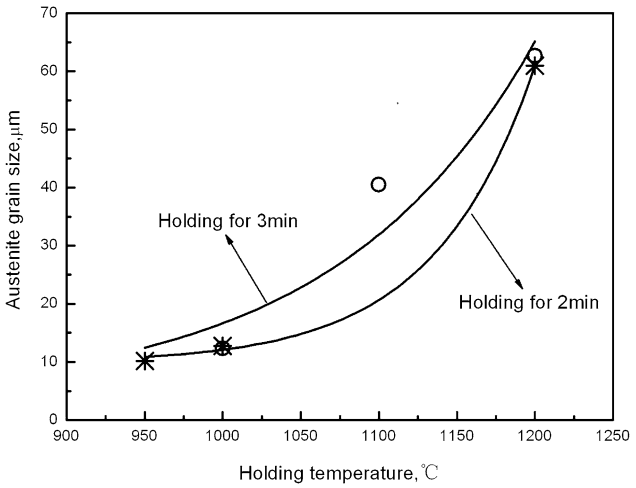

Fig. 1 Effect of reheating condition on austenite grain size (steel A)

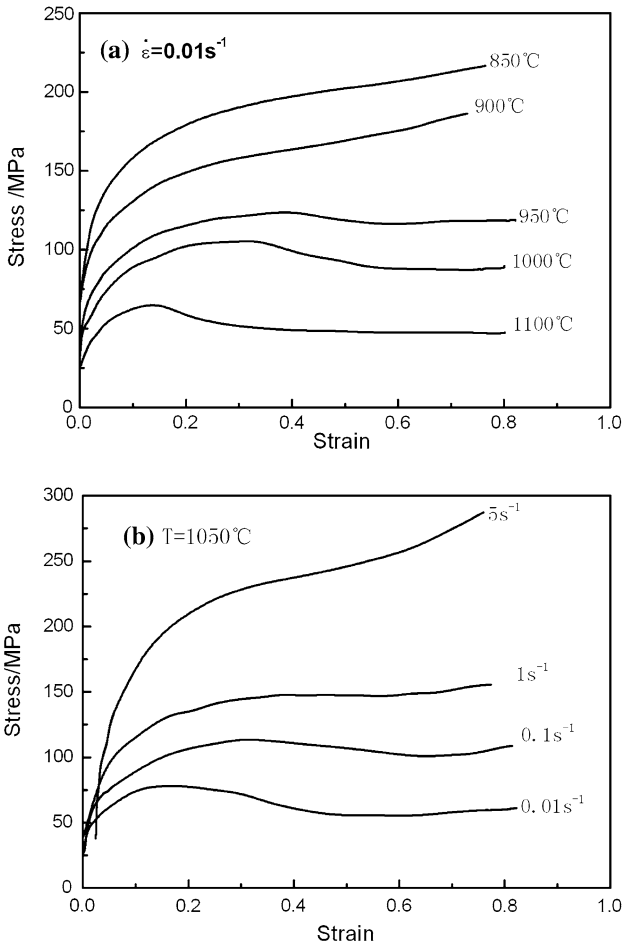

Fig. 2 Effect of temperature (**a**) and strain rate (**b**) on the stress–strain curve (steel A)

and at strain rates in the range from 0.01–10 s^{-1}. Under low temperatures or high strain rates, the flow stress increases with increasing strain and shows the characteristic of work-hardening and dynamic recovery. With increasing deformation temperature and/or decreasing strain rate, DRX occurs in the recorded stress–strain curve, which displayed a rapid increase to a maximum stress, characterized by a peak strain and peak stress, followed by a gradual fall to a steady state stress. Furthermore, the values for peak strain, peak stress, and steady state stress increases with a decrease in deformation temperature and/or an increase in strain rate. A typical kinetic relationship is usually expressed by the following equation [24]:

$$\dot{\varepsilon} = A[\sinh(\alpha\sigma)]^{\lambda}\exp\left(-\frac{Q_d}{RT}\right) \quad (1)$$

$$Z = \dot{\varepsilon}\exp\left(\frac{Q_d}{RT}\right) \quad (2)$$

where A, α, and n are constants, Q_d is the deformation activation energy, Z the Zener–Hollomon Parameter [24], $\dot{\varepsilon}$

the strain rate, σ the stress, R the universal gas constant, and T is the absolute temperature. Eq. 1 can also be approximated by the power relation:

$$\dot{\varepsilon} = B\sigma^{\lambda} \exp\left(\frac{-Q_d}{RT}\right) \tag{3}$$

where B and λ are constants.

For this high-Nb steel studied, the value for λ at the peak was estimated 6.4, utilizing the linear relationship between the natural logarithm of σ and $\dot{\varepsilon}$ as shown in Fig. 3a.The deformation activation energy for the peak stress of DRX, which is here also called as the activation energy for DRX, was determined to be 373 kJ/mol, as illustrated in Fig. 3b. This value is higher than the self-diffusion energy in austenite (270 kJ/mol) and that of low carbon steels being approximately 300 kJ/mol or below as a result of solute strengthening by Mn or Si. The deformation activation energy in low-Nb microalloyed steels that have been shown to undergo DRX is generally somewhat higher (about 330 kJ/mol or above) than those of C steels because of the presence of solute and microalloying carbonitrides

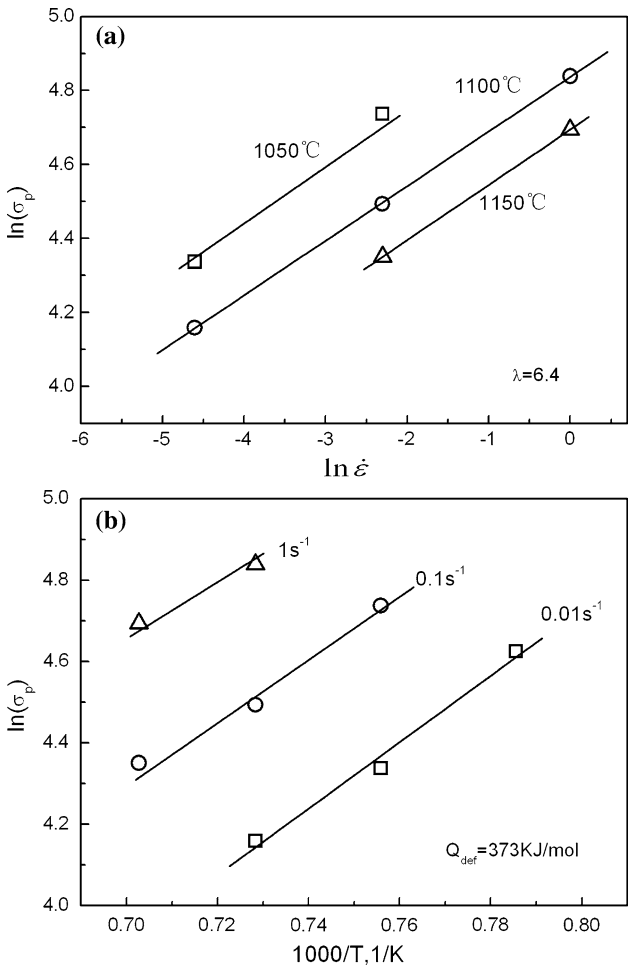

Fig. 3 Determination of λ (**a**) and Q_d (**b**) values in Eqs. 1 and 3 (steel A)

[25]. Of course, there are also higher values (above 400 kJ/mol) of deformation active energy reported in other Nb-containing steels, which is probably associated with the experimental data used to estimate the active energy. When these cases that dose not undergo DRX are involved in this analysis, the estimated values of active energy appear to be higher.

Critical strain for the initiation of DRX

The peak strain ε_p is often described as a power function of Z

$$\varepsilon_p = CD_0^p Z^b \tag{4}$$

where D_0 is the initial grain size, C, p, and b are material constants. The linear relationship between the natural logarithm of ε_p and Z in high-Nb steel is shown in Fig. 4. As we know, DRX is initiated not at the peak strain ε_p but at a critical strain ε_c below ε_p, and even in some cases, no clearly defined stress and strain peaks are observed in flow curves. Thus, it is of most interest to determine the critical strain for DRX in the mathematical modeling of microstructural evolution. Ryan and McQueen [26] have reported that the presence of a stress peak in a constant strain rate flow curve leads to an inflection in the stress dependence of the strain hardening rate, $\theta = (\partial\sigma/\partial\varepsilon)_{\dot{\varepsilon}}$. Later, it is also repeatedly confirmed by irreversible thermodynamics and the observations in many materials that the inflections in θ–σ or In θ–In σ plots can serve as indications of DRX [27–29]. Accordingly, the critical strains in the three steels investigated here are determined from the inflection points of the $\ln\theta - \ln\sigma$ plots as shown in Fig. 5. The corresponding $\varepsilon_c/\varepsilon_p$ ratios together with those reported by Siciliano and Jonas [30] as a function of the effective Nb concentration (Nb_{eff}) are summarized in Fig. 6, in which Nb_{eff} is represented as

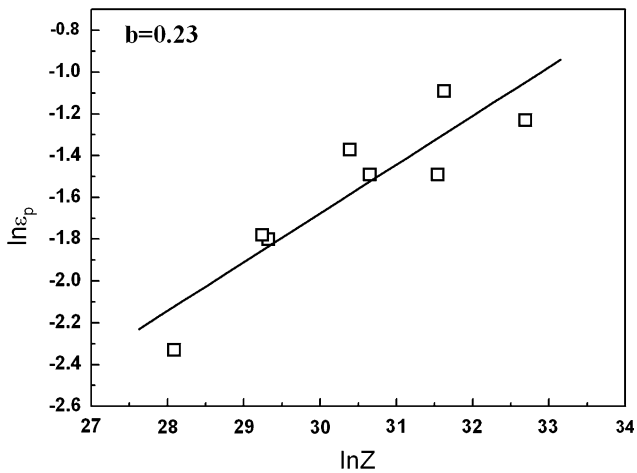

Fig. 4 Relationship between the peak strain and the Zener–Hollomon parameter (steel A)

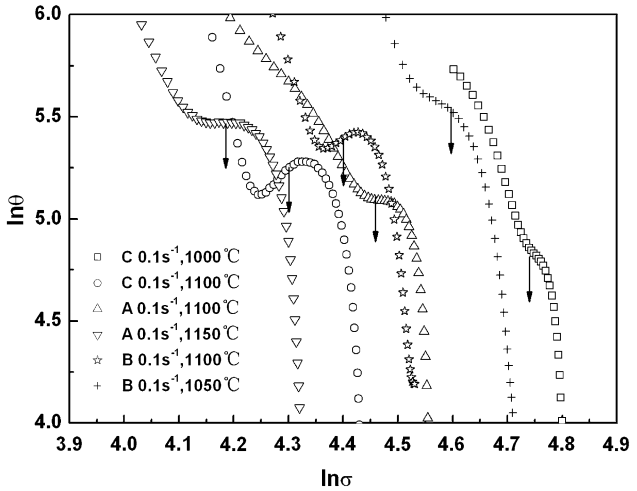

Fig. 5 Dependence of the strain hardening rate on the stress at different conditions

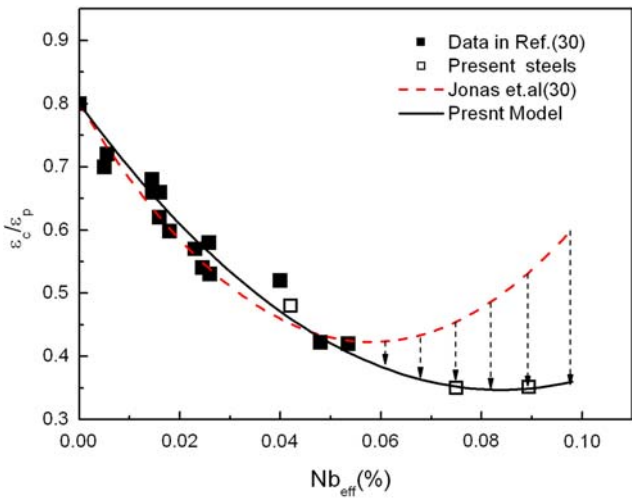

Fig. 6 Relationship between the $\varepsilon_c/\varepsilon_p$ ratio and the effective Nb concentration

$$Nb_{eff} = Nb - Mn/120 + Si/94 \quad (5)$$

where the effects of Mn and Si contents (in weight percent) are taken into account in addition to Nb content. It can be seen that, there exists a clear relationship between the $\varepsilon_c/\varepsilon_p$ ratio and the effective Nb concentration, i.e., the $\varepsilon_c/\varepsilon_p$ ratio exhibits a deceasing tendency with increasing the Nb_{eff} content. However, the fit equation proposed by Siciliano and Jonas [30] is only available to the relatively low Nb_{eff} contents, i.e., smaller than 0.06% (see Fig. 6), and there is a large deviation between these predictions (dash line) and measurements for the higher Nb_{eff} content (e.g., steels A and B). That is to say, the $\varepsilon_c/\varepsilon_p$ ratio is observed for high-Nb steels as low as approximately 0.35 and tends to a constant when Nb_{eff} content reaches as high as about 0.1. This is quite different from the traditional Nb-containing steels where the ratios often lie in between 0.4 and 0.8. It is also suggested that high-Nb material exhibits the stronger effect of retarding the DRX progress, and this effect is gradually stabilized when the Nb_{eff} content is high enough. Hence, a new fit equation capable of being applied over the wider range of Nb_{eff} content is given as

$$\varepsilon_c/\varepsilon_p = 0.8 - 10.8Nb_{eff} + 64.4Nb_{eff} \quad (6)$$

Static recrystallization

Double-hit compressive tests are commonly conducted to monitor the SRX behavior. By allowing a relaxation time after the first hit, static recovery and SRX take place in the material. The recrystallized fraction (X_f) after an interval of hot deforming was determined using the "back extrapolation" method by analyzing experiment data [31, 32], as shown in Fig. 7. Clearly, the softening rate increases with the increase in deformation temperatures, which is attributable to the higher mobility of grain boundaries at elevated temperatures. For example, at 1050 °C the softening curves follow Avrami's law for all the samples tested here. As deformation temperature decreases, a plateau can be observed in many cases whether for steel A or D. This plateau is a consequence of strain-induced precipitation. It is well known that the addition of Nb retards recrystallization by the solute drag and pinning of strain-induced precipitates. Solute drag will alter the rate of softening, whereas strain-induced precipitation has a much stronger influence and effectively stops recrystallization for a relatively long time. The temperature and time where the plateau starts to appear depend on all the variables that intervene in hot deformation, including the chemical composition of the steel. As illustrated in Fig. 7a, recrystallization in steel A is thought to nearly end below 950 °C for the first hit strain of 0.3 in the range of interpass times tested, 1–400 s. Recrystallization can be promoted by heightening the applied strain from 0.3 to 0.5 because of the corresponding increase in driving force for recrystallization to take place. But in steel D, the recrystallization fraction is still close to 50% at deformation temperature of 900 °C and the interpass time of 400 s, despite the plateau observed in softening curve previously. Steel A contains higher Nb when compared to Steel D and thus it is likely that relatively more strong effect of retarding the recrystallization can be seen in steel A. Further, the recrystallization rate increases with decreasing austenite grain sizes resulting from different austenitization conditions, as illustrated in Fig. 7c. This reflects an increase in grain boundaries, as preferred nucleation sites of new recrystallized grain, when austenite grain is refined.

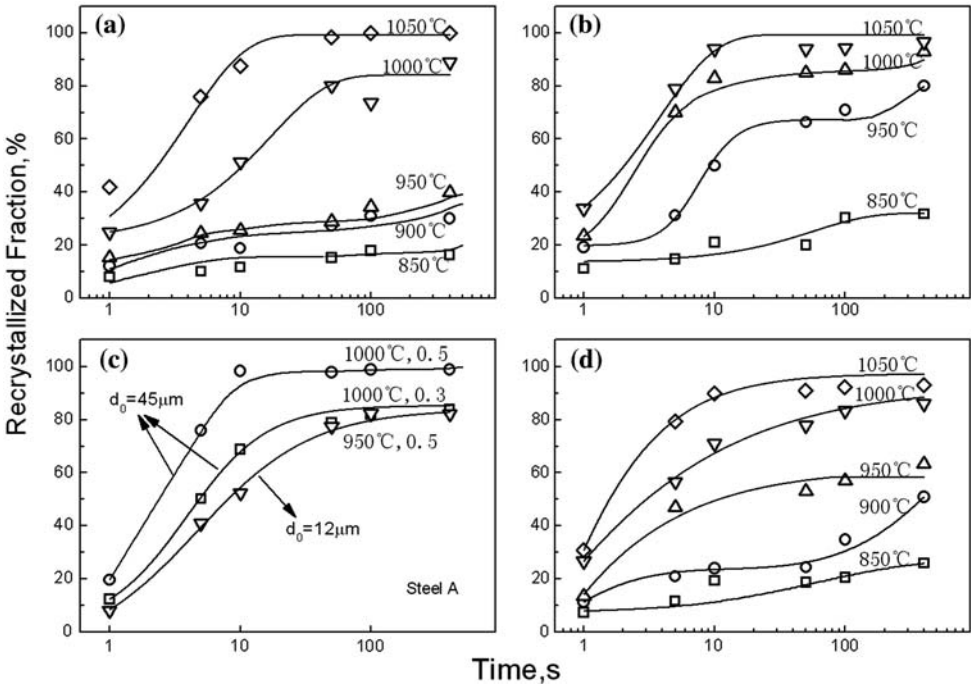

Fig. 7 Static softening kinetics curves of high-Nb steels under various conditions **a** steel A, $d_0 = 64$ μm, $\varepsilon = 0.3$; **b** steel A, $d_0 = 64$ μm, $\varepsilon = 0.5$; **c** steel A, $d_0 = 45$ or 12 μm; **d** steel D, $d_0 = 64$ μm, $\varepsilon = 0.3$

The recrystallization kinetics can be described using a form of the Avrami equation [18]:

$$X = 1 - \exp\left[-0.693\left(\frac{t}{t_{0.5}}\right)^{k}\right] \tag{7}$$

where X is the recrystallized fraction, t is time (s), k is the Avrami constant and $t_{0.5}$ is the time for 50% recrystallization. The parameter $t_{0.5}$ can be represented by a function of temperature (T), initial austenite grain size (d_0), applied strain (ε) such that

$$t_{0.5} = A_1 \varepsilon^{A_2} d_0^{A_3} \exp(Q_{\text{rex}}/RT) \tag{8}$$

where Q_{rex} is the apparent activation energy for recrystallization, A_1, A_2, A_3 are constants. The parameters for the time of 50% recrystallization are summarized in Table 2 together with the Avrami constant k for the present steels A and D, which were determined using line regression method, as illustrated in Figs. 8 and 9. The values of A_1, A_2, A_3, and k as well as Q_{rex} basically fall into the range of the corresponding ones reported for the recrystallization kinetics of other Nb-HSLA steels [33]. However, the Q_{rex} value is also found to have a large difference in the two steels, i.e., the Q_{rex} value in steel A is much greater than that in steel D, which is most likely due to the more effective solute drag in high-Nb steel when compared to low-Nb steel. In other words, the increase of the Nb content in steel would result in a greater difficulty for the austenite to recrystallize. It should be noted that the value of activation energy approximately remains constant before the precipitation takes place, and once the strain-induced precipitation is initiated, this value increases significantly, which means that the recrystallization stops for a relatively long time until the pinning effective is eliminated with the coarsening of precipitated particles. A reasonable agreement between the predicted and the experimental ones can be obtained as shown in Fig. 10.

Table 2 Parameters for static recrystallization in Eqs. 7 and 8

Steel	A_1	A_2	A_3	k	Q_{rex} (kJ/mol)
A	7.22×10^{-18}	−1.4	2.1	0.6	331
D	1.64×10^{-11}	−2.0	1.1		205

Interaction of precipitation and recrystallization

The strain-induced precipitation of the high-Nb microalloyed steel here was estimated using a model based on the precipitation start model of Dutta and Sellars, shortened as D–S model [34]. This model predicts the starting time for precipitation, i.e., the time for 5% precipitation, under isothermal conditions using the following equation:

$$t_{ps} = A[Nb]^{-1}\varepsilon^{-1}Z^{-0.5}\exp\left(\frac{270000}{RT}\right)\exp\left[\frac{B}{T^3(\ln k_s)^2}\right] \tag{9}$$

where the supersaturation ratio $k_s = ([\text{Nb}][\text{C} + 12\ \text{N}/14])/10^{2.26-6770/T}$, [Nb], [C], and [N] are the weight percentages of Nb, C, and N, respectively, Z is the Zener–Hollomon parameter, ε the applied strain, T the temperature (in K) and A, B are constants which can determined by fitting the

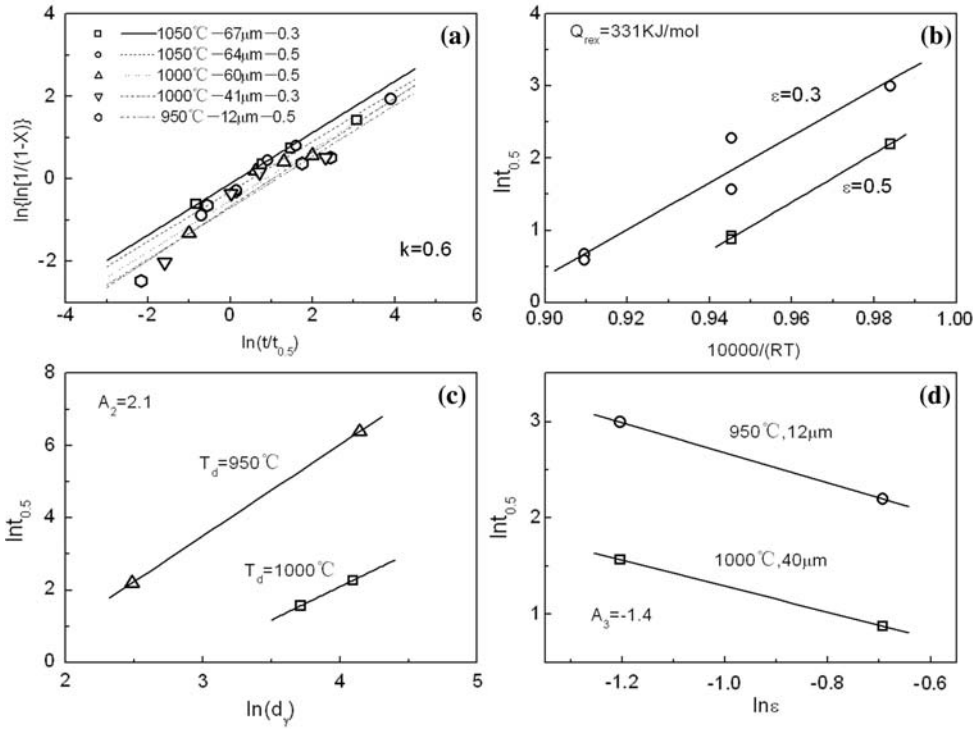

Fig. 8 Determination of relative coefficients in Eqs. 7 and 8 for steel A. **a** $k = 0.6$, **b** $Q_{rex} = 331$ kJ/mol; **c** $A_2 = 2.1$; **d** $A_3 = -1.4$

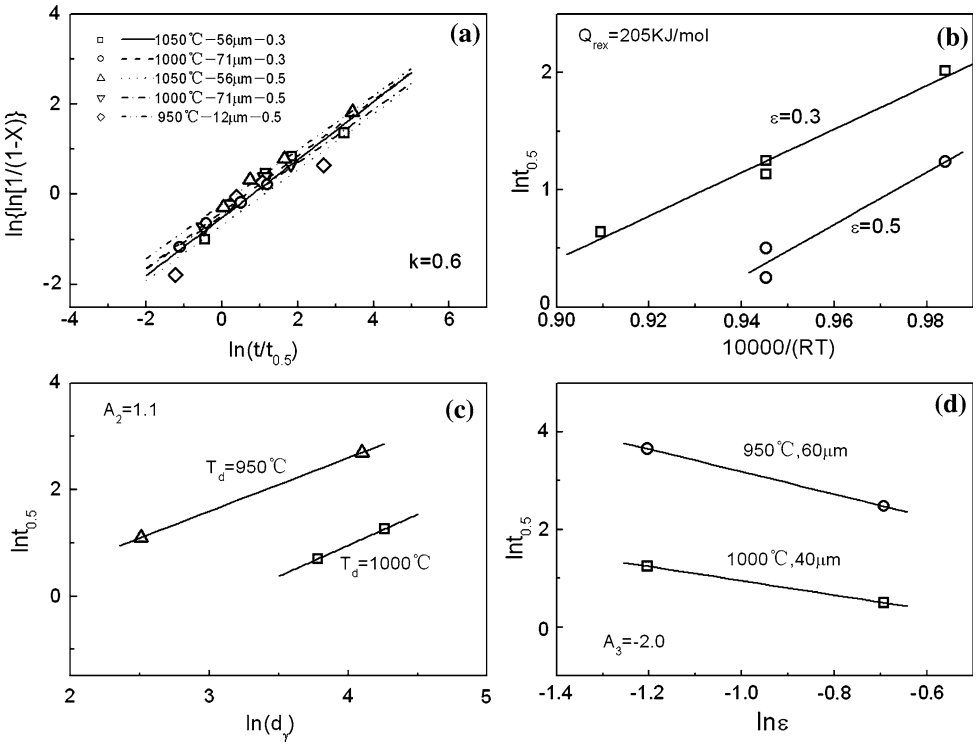

Fig. 9 Determination of relative coefficients in Eqs. 7 and 8 for steel D. **a** $k = 0.6$, **b** $Q_{rex} = 205$ kJ/mol, **c** $A_2 = 1.1$, **d** $A_3 = -2.0$

experimental data. The effect of strain rate on precipitation times is taken into account in the Zener–Hollomon parameter as a function of strain rate, as given in Eq. 2. Dutta and Sellars [34] used the mean values of $Q_{def} = 400$ kJ/mol, $A = 3 \times 10^{-6}$, and $B = 2.5 \times 10^{10}$ in modeling the precipitation kinetics of Nb-bearing steels.

Figure 11 shows the calculated precipitation–temperature–time (PTT) curves with the strains of 0.3 and 0.5 and some measured points. Here, the measured ones can be obtained by analyzing TEM micrographs of strain-induced precipitation and the experimental data associated with the plateau exhibited in the softening curves.

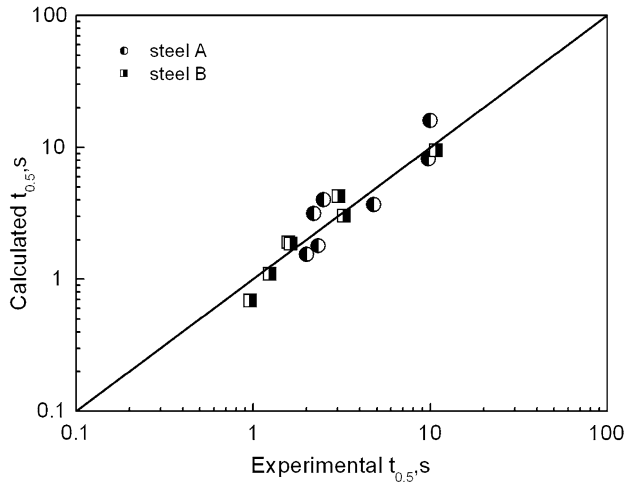

Fig. 10 Predicted $t_{0.5}$ according to Eq. 8 versus experimental $t_{0.5}$ for the present steels

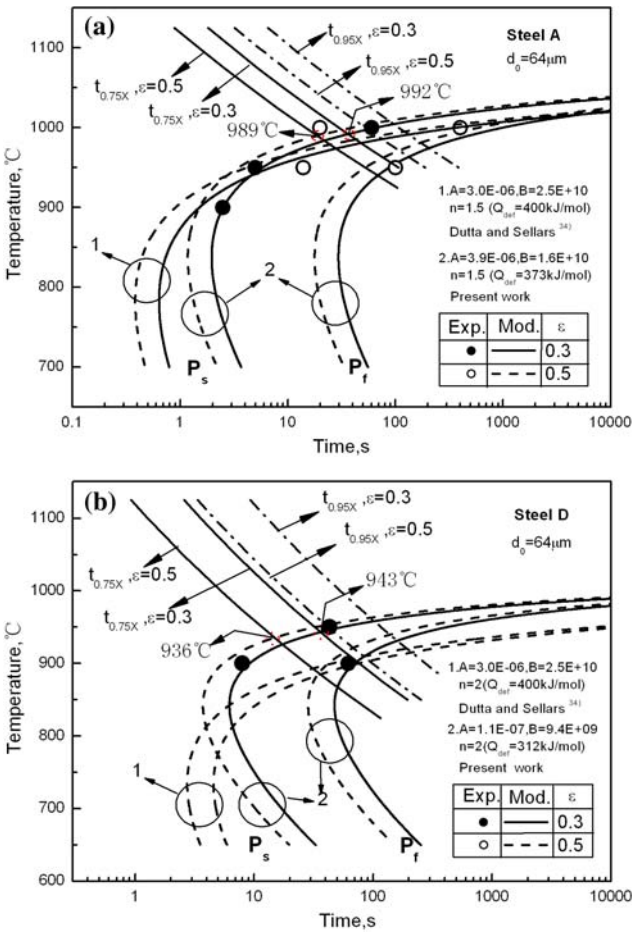

Fig. 11 Calculated strain-induced precipitation and recrystallization kinetics **a** steel A and **b** steel D

The finishing time (P_f) of the strain-induced precipitation that is also the time to 95% precipitation was calculated by

$$X_P = 1 - \exp\left[-\ln(0.95)\left(\frac{t}{t_{ps}}\right)^n\right] \quad (10)$$

This equation is an extension to the D–S model, using a modified Avrami equation to estimate the volume fraction of precipitate that formed as a function of time. Where, X_P is the volume fraction of precipitate, t_{ps} is the precipitation start time at the present temperature and n is the Avrami exponent. For the present steels A and D, the values of $Q_{def} = 373$ and 312 kJ/mol have been, respectively, determined as mentioned above, and thus these values must be considered in the calculation of the precipitation times. Taking it into account, the following new values of the constants have been calculated for a better fit with experimental observations, $A = 3.9 \times 10^{-6}$, $B = 1.6 \times 10^{10}$, $n = 1.5$ for steel A, and $A = 1.1 \times 10^{-7}$, $B = 9.4 \times 10^{9}$, $n = 2.0$ for steel D. The calculated precipitation times are shown in Fig. 11. The precipitation start and end times calculated from Eqs. 9 and 10, using these values of the constants and activation energy, show a more reasonable agreement with the experimental points than using the corresponding values proposed by Dutta and Sellars [34]. By comparing PTT curves in these two steels, it can also be seen that, the nose of precipitation in steel A, situates in a temperature range from about 700 to 900 °C, corresponding to the precipitation times of 1–4 s, while the nose temperature of 800–900 °C and the shortest precipitation times of 4–10 s are observed in steel D. Figure 12 shows the TEM replica micrographs of NbC precipitates and corresponding Energy Dispersive X-Ray Spectrum (EDXS) result. Here, the deformation temperature is 900 °C, the stain rate is 5 s^{-1}, and the pre-strain is about 0.3. After deformation, the sample is held for 100 s before quenching.

In order to model the interaction between the precipitation and recrystallization, the times calculated by the present recrystallization models (Eqs. 7 and 8) to reach a 75 and 95% recrystallized fraction after deformation at a given strain has been plotted in the same figure. Noting that, the kinetics of recrystallization and precipitation are modeled separately. Here, two important concepts have to be mentioned, i.e., the recrystallization limit (RLT) and recrystallization stop (RST) temperatures. The two temperatures are, respectively, defined by Dutta and Sellars [34] as the lowest temperature above which recrystallization is complete (85 or 95% recrystallization criteria have been used) and the highest temperature at which recrystallization is completely absent (usually the criteria of 5% recrystallization is considered). Another concept widely used in designing controlled rolling schedules is the non-recrystallization temperature (T_{nr}) below which strain is accumulated in the austenite (pancaking).This temperature is also affected by the interaction between the deformation, recrystallization, and precipitation. Abad et al. [35] have,

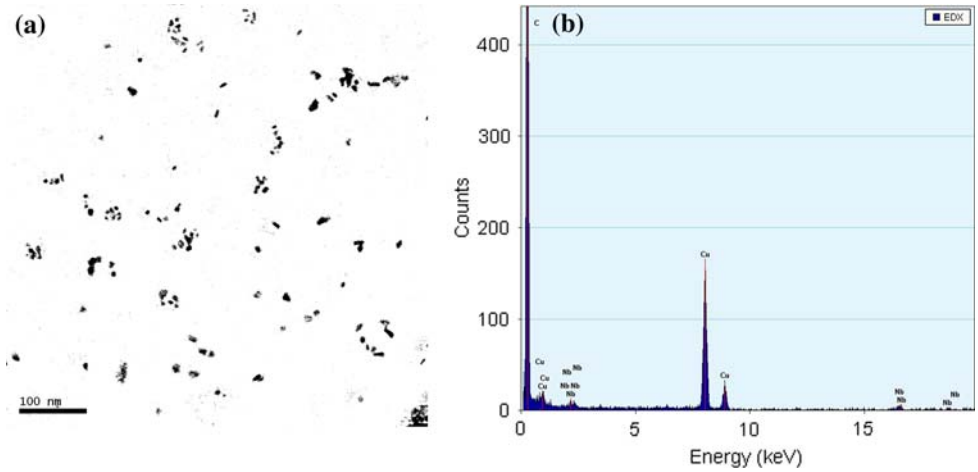

Fig. 12 TEM replica micrographs and corresponding EDXS spectra showing NbC precipitates in steel A (holding time of 100 s after deformation at 900 °C)

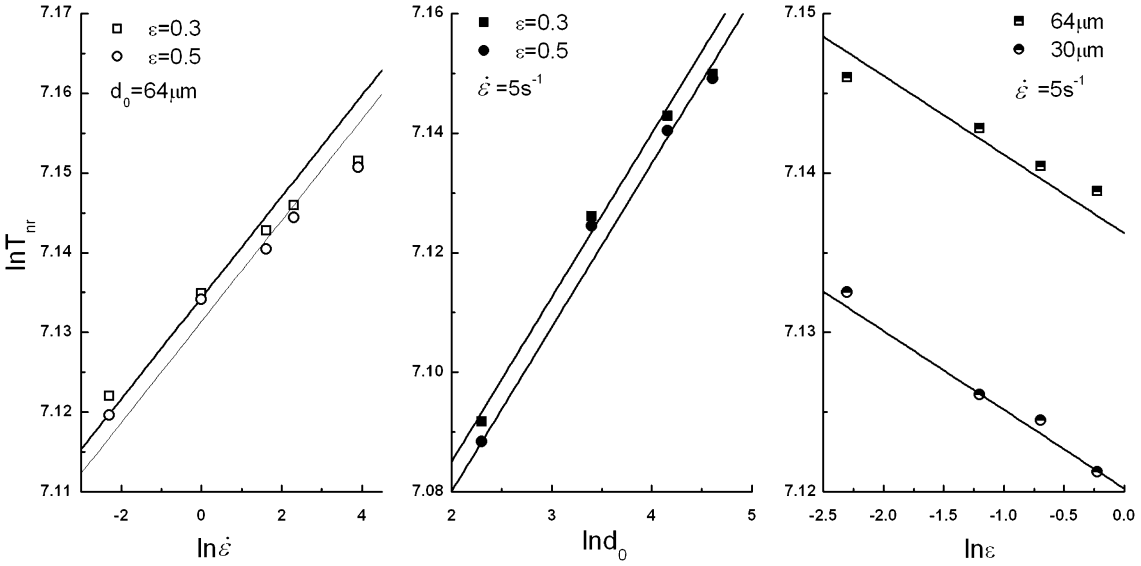

Fig. 13 Dependence of T_{nr} on strain rate (ε), grain size (d_0) and strain ($\dot{\varepsilon}$) in steel A

respectively, measured the T_{nr}, RLT, and RST temperatures in a low-Nb microalloyed steel based on mutipass torsion tests performed under continuous cooling conditions and proposed that the T_{nr} values are always located between RLT and RST temperatures, but dose not exactly represent the temperature above which the recrystallization is complete. For example, the amount of softening reached to the T_{nr} temperature ranges from 63 to 78% for the strain of 0.2–0.4. A similar phenomenon was also observed in other works [36, 37]. Therefore, in the present work, we may adopt the criteria of 75% recrystallization to simply evaluate the non-recrystallization temperature using the recrystallization–precipitation interaction diagram (see Fig. 11), which is similar to the determination of RLT and RST temperatures proposed by Dutta and Sellars [34]. That is to say, when the time for 75% recrystallization ($t_{0.75X}$) becomes equal to the time for 5% strain-induced precipitation (t_{ps}) the T_{nr} temperature is thought to be reached. As a consequence, for a strain of $\varepsilon = 0.3$ and austenite grain size of $d_0 = 64$ μm, the T_{nr} temperatures of 992 and 943 °C are, respectively, obtained in steels A and D. It is also seen that the T_{nr} in steel A appears to be about 30 °C higher than that reported by Bai et al. [38] for another high-Nb steel tested under continuous cooling conditions. This can be explained by the fact that relatively long interpass times (30 s) and gradually refined austenite grain (probably much smaller than 64 μm in the later passes) promote greatly recrystallization between passes, leading to a reduction in the time for 75% recrystallization. Additionally, the high-Nb steel has a higher T_{nr} value than the low-Nb steel and the difference between both is of about 50 °C. This further proves that high-Nb steels have a boarder non-recrystallization temperature window, but the extent of this window is not invariable but affected by

many factors such as chemical composition, processing parameters, and microstructural variables. As an example, Fig. 13 gives the logarithmic plot showing the dependence of T_{nr} on strain (ε), grain size (d_0), and strain ($\dot{\varepsilon}$) in steel A. This relationship can be summarized as the following equation:

$$T_{nr} = 1109\varepsilon^{-4.9\times10^{-3}}\dot{\varepsilon}^{6.3\times10^{-3}}d_0^{2.7\times10^{-2}}\ (\text{in Kelvin}) \qquad (11)$$

In fact, the interpass interval time is another crucial factor affecting the T_{nr} especially in commercial rolling. As we know, the SRX kinetics is highly time-dependent and thus, even in absence of strain-induced precipitation, in the case of short interpass interval, it becomes very difficult for fully recrystallization to take place, i.e., a T_{nr} can still be obtained. This is explained as a result of the retardation of recrystallization by solute drag effect in Bai et al.'s work [38]. Actually, even for plain carbon steels, as long as the interpass interval is enough short, there is still non-recrystallization phenomenon found particular in the later passes of Hot-strip mill (HSM).Thus, the estimation of T_{nr} during interpass interval of hot rolling is fairly complex. Although the mean flow stress (MFS) in each pass is also used to reflect the metallurgical characteristics such as solute effect, strain accumulation, and recrystallization, it is difficult to be measured accurately in industrial conditions. Clearly, only the softening fraction between passes is most available for the determination of T_{nr} in practical rolling.

Conclusions

Based on laboratory simulations, an overall microstructural model describing recrystallization and precipitation has been proposed for hot-strip rolling of an ultralow-carbon, high-Nb HSLA steel. The model represents a first extension of approaches previously proposed for plain carbon and low-Nb HSLA steels and can be used to evaluate the effects of modifications to processing parameters in industrial conditions. The following conclusions are drawn from this work:

(1) The present high-Nb steel has a deformation active energy of 373 kJ/mol, which is usually higher than those in low carbon and low-Nb microalloyed steels that have been shown to undergo DRX attributable to the effect of high level of Nb addition. Similarly, the high SRX active energy (330 kJ/mol) can lead to a greater difficulty for the austenite to recrystallize.

(2) The $\varepsilon_c/\varepsilon_p$ ratio was observed for high-Nb steels as low as approximately 0.35 and tends to constant when Nb_{eff} content ranges from 0.07 to 0.10. This is quite different from the traditional Nb-containing steels where the ratios often fall into the range of 0.4–0.8. Hence, a new fit equation capable of being applied over the wider range of Nb_{eff} content is given as $\varepsilon_c/\varepsilon_p = 0.8 - 10.8Nb_{eff} + 64.4Nb_{eff}$.

(3) Taking the Q_{def} values determined in the present paper into account, the following new values of the constants in the starting precipitation equation proposed by Dutta and Sellars were calculated for a better fit with experimental observations, $A = 3.9 \times 10^{-6}$, $B = 1.6 \times 10^{10}$ for high-Nb steel and $A = 1.1 \times 10^{-7}$, $B = 9.4 \times 10^{9}$ for low-Nb steel.

(4) The recrystallization–precipitation interaction diagram was used to simply evaluate the non-recrystallization temperature (adopting the criteria of 75% recrystallization). For the case of a strain of 0.3 and austenite grain size of 64 μm, the T_{nr} temperature of high-Nb steel is around 50 °C higher than that of the low-Nb steel. Moreover, a new equation representing the effects of strain, grain size, and strain rate on T_{nr} in high-Nb steel has been first summarized as $T_{nr} = 1109\varepsilon^{-4.9\times10^{-3}}\dot{\varepsilon}^{6.3\times10^{-3}}d_0^{2.7\times10^{-2}}$ (in Kelvin).

Acknowledgements This work was financially supported by the National Natural Science Foundation of China (No. 50504007), the Fundamental Research Funds for the Central Universities (N090407001) and the National Key Project of Scientific and Technical Supporting Programs (No. 2007BAE51B07). This work also was supported by Benxi Iron & Steel Corp., China.

References

1. Kim NJ, Thomas G (1981) Metall Trans 12A:483
2. Kim NJ, Thomas G (1984) Scr Metall 18:817
3. Baczynski GJ, Jonas JJ, Collins LE (1999) Metall Mater Trans 30A:3045
4. Bakkaloğlu A (2002) Mater Lett 56:200
5. Kong JH, Zhen L, Guo B, Li P et al (2004) Mater Des 25:723
6. Zhao MC, Yang K, Shan YY (2002) Mater Sci Eng 335 A:14
7. Zhao MC, Yang K, Xiao FR, Shan YY (2003) Mater Sci Eng 355 A:126
8. Araki T et al (1992) Continuous-cooled Zw microstructures of low-carbon steel. ISIJ, Tokyo, p 4
9. Xiao F, Liao B, Ren D et al (2005) Mater Charact 54:305
10. Koo JY, Luton MJ, Bangaru NV, Petkovic RA (2003) Proceedings of 13th international offshore and polar engineering conference, vol 4, p 10
11. Korczak P, Dyja H, Pilarczyk JW (1998) Met Mater Int 4:707
12. Manohar PA, Chandraand T, Killmore CR (1996) ISIJ Int 36:1486
13. Suehiro M, Liu Z-K, Ågren J (1996) Acta Mater 44:4241
14. Suehiro M (1998) ISIJ Int 38:547
15. Hulka K, Bordigon P, Gray M (2006) Microalloy Technol 6:1
16. Stalheim DG, Barnes KR, Mccutcheon DB (2006) Microalloy Technol 6:15
17. Umemoto M, Hiramatsu A, Moriya A et al (1992) ISIJ Int 32:306
18. Fernández AI, Uranga P, López B, Rodriguez-Ibabe JM (2000) ISIJ Int 40:893

19. Kern A, Degenkolbe J, Müsgen B, Schriever U (1992) ISIJ Int 32:387
20. Yoshie A, Fujioka M, Watanabe Y et al (1992) ISIJ Int 32:395
21. Umemoto M, Nishioka N, Tamura I (1981) J Heat Treat 2:121
22. Shin DH, Kim BC, Kim YS, Park KT (2000) Acta Mater 48:2247
23. Saito Y, Shiga C, Enami T (1988) THERMEC-88. ISIJ, Tokyo, p 753
24. Poliak EI, Jonas JJ (2003) ISIJ Int 43:684
25. McQueen HJ, Yue S, Ryan ND, Fry E (1995) J Mater Process Technol 53:293
26. Ryan ND, McQueen HJ (1990) J Mater Process Technol 8:177
27. Poliak EI, Jonas JJ (1996) Acta Metall Mater 44:127
28. Manonukul A, Dunne FPE (1999) Acta Mater 47:4339
29. Kim SI, Yoo YC (2002) Mater Sci Technol 18:160
30. Siciliano F Jr, Jonas JJ (2000) Metall Mater Trans 31A:511
31. Medina SF, Quispe A (2001) ISIJ Int 41:774
32. Andrade HL, Akben MG, Jonas JJ (1983) Metall Trans 14:1967
33. Militzer M, Hawbolt EB, Meadowcroft TR (2000) Metall Mater Trans 31 A:1247
34. Dutta B, Sellars CM (1987) Mater Sci Technol 22:217
35. Abad R, Fernández AI, López B, Rodriguez-Ibabe JM (2001) ISIJ Int 41:1373
36. Radovic N, Drobnjak D (1999) ISIJ Int 39:575
37. Medina SF (1998) Mater Sci Technol 14:217
38. Bai DQ, Yue S, Sun WP, Jonas JJ (1993) Metall Trans 24A:2151